REPORT

SOLAR PHYSICS

Decay of the coronal magnetic field can release sufficient energy to power a solar flare

Gregory D. Fleishman[1]*, Dale E. Gary[1], Bin Chen[1], Natsuha Kuroda[2,3], Sijie Yu[1], Gelu M. Nita[1]

Solar flares are powered by a rapid release of energy in the solar corona, thought to be produced by the decay of the coronal magnetic field strength. Direct quantitative measurements of the evolving magnetic field strength are required to test this. We report microwave observations of a solar flare, showing spatial and temporal changes in the coronal magnetic field. The field decays at a rate of ~5 Gauss per second for 2 minutes, as measured within a flare subvolume of ~10^{28} cubic centimeters. This fast rate of decay implies a sufficiently strong electric field to account for the particle acceleration that produces the microwave emission. The decrease in stored magnetic energy is enough to power the solar flare, including the associated eruption, particle acceleration, and plasma heating.

The solar corona sometimes exhibits an explosive release of the energy stored in magnetized plasma, which drives phenomena such as solar flares (*1*–*5*). The standard model of solar flares (*6*–*9*) posits that they are powered by magnetic energy stored in the solar corona and released (dissipated into other forms) through magnetic reconnection (*10*)—a reconfiguration of the magnetic field topology toward a state of lower magnetic energy. Changes in the coronal magnetic field during a flare or other large-scale eruption have been quantified only indirectly, for example (*11*), from extrapolations of the magnetic field measured at the photosphere—the surface layer of the Sun seen in white light. Although this method can quantify the modest magnetic energy transfer of ~10%, it is known to suffer from many shortcomings (*12*). The extrapolation approach does not allow the dynamic local changes of the magnetic field to be quantified at time scales short enough to characterize the flare energy release.

We report observations (*13*) of a large solar flare—one of several that occurred in September 2017. The partially occulted eruptive flare occurred in active region (AR) 12673, at heliographic coordinates 9° south, 91° west (Fig. 1A), on 10 September 2017. This event exhibits the main ingredients of the standard flare model, including a cusplike structure of nested magnetic loops that evolves upward at a speed of ~30 km s^{-1} and an apparent current sheet (Fig. 1A) (*14*–*16*). This eruptive flare was widely observed at many wavelengths (*14*–*19*). Estimates of the kinetic, thermal, and nonthermal energies released in the flare are available from complementary approaches and datasets, whereas the dominant magnetic energy has only been estimated indirectly (*20*). Figure 1 shows context information for the flare, including the microwave images that we observed using the Expanded Owens Valley Solar Array (EOVSA) (*21*) in 26 microwave bands in the range of 3.4 to 15.9 GHz (*13*).

We produced magnetic field maps from these observations (*13*), examples of which are shown in Fig. 2. The full sequence is shown in movie S1. They show strong variation between maps, demonstrating the fast evolution of the coronal magnetic field strength B. The magnetic field strength decays quickly at the cusp region; away from that region, the field also decays but more slowly.

To quantify this decay, Fig. 3 shows the time evolution of the flaring coronal magnetic field at two locations marked in Fig. 2. Both locations exhibit a decay in the magnetic field strength but with different timing. One location shows a decay of the magnetic field from ~600 to ~200 G over ~1 min, a magnetic field decay rate of $|\dot{B}| \approx 6.6\ \mathrm{G\ s^{-1}}$. The decay ends at about 15:58 Coordinated Universal Time (UTC), after which the magnetic field at this location remains roughly constant. By contrast, the location within a larger and higher collapsing loop, marked in Fig. 1A, experiences a longer decay, until roughly 16:00 UTC. In this location, the magnetic field decays from ~900 to ~250 G over ~2 min, a rate of $|\dot{B}| \approx 5.4\ \mathrm{G\ s^{-1}}$. The energy release suggested by this magnetic

[1]Center for Solar Terrestrial Research, New Jersey Institute of Technology, University Heights, Newark, NJ 07102, USA. [2]University Corporation for Atmospheric Research, Boulder, CO 80307, USA. [3]Space Science Division, Code 7684, Naval Research Laboratory, Washington, DC 20375, USA.
*Corresponding author. Email: gfleishm@njit.edu

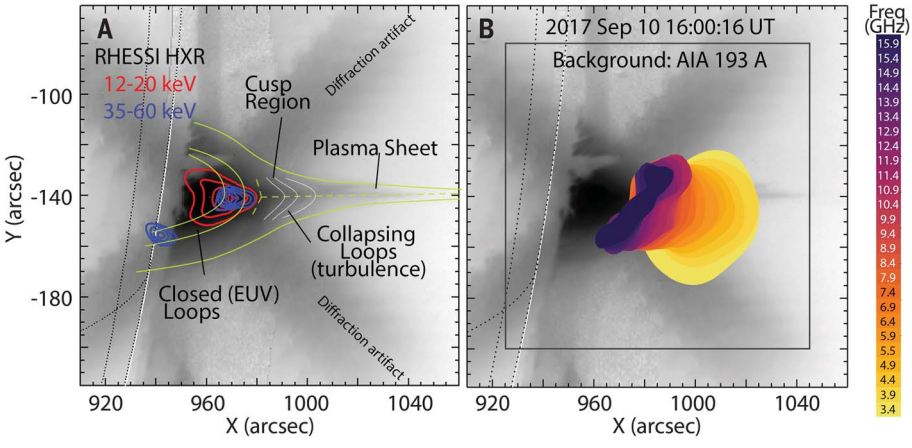

Fig. 1. Multiwavelength observations of the class X8 flare on 10 September 2017. (**A**) An EUV image (193 Å) with inverted brightness overlain with contours outlining the thermal (red contours) and nonthermal (blue contours) hard x-ray (HXR) emission (*16*). The green and white lines are a schematic drawing of the plasma sheet (the current sheet, according to the standard solar flare model), closed and collapsing (newly reconnected) loops, and the cusp region, where the fastest evolution of the magnetic field takes place. Only one of the loop foot points (the southern one) is located on the visible side of the disk, whereas the other is located behind the limb (occulted by the Sun). The thin white curve shows the solar surface (photosphere). The dotted black lines indicate the solar coordinate grid marked at 5° intervals. X and Y are the Cartesian coordinates with the coordinate center adopted in the center of the solar disk. RHESSI, Reuven Ramaty High Energy Solar Spectroscopic Imager. (**B**) The same image as (A), overlain with the microwave observations taken with EOVSA. The colored regions indicate the ≥50% brightness areas corresponding to 26 frequencies from 3.4 to 15.9 GHz. The relationships among different data sources suggest that the microwave emission comes from the cusp region, outlining the newly reconnected collapsing field lines. The gray box outlines the region of corresponding magnetic field maps in Fig. 2. AIA, Atmospheric Imaging Assembly; Freq., frequency.

field decay ends around the time of the peak microwave emission (16:00 UTC), which is consistent with the theoretical predictions of microwave emission arising from a population of trapped electrons (*16*).

We compare these measurements of the decaying coronal magnetic field with equilibrium models that are based on extrapolation of photospheric magnetic field measurements (*11*). The extrapolation requires corresponding photospheric vector magnetic field data, which are not available for this partially occulted event. However, magnetic field models are available (*22*) for this AR a few days earlier, on 6 September 2017, when this AR could be seen more face-on. These models found that the strongest magnetic field in the corona at the height of 30 Mm was ~200 G [figure 5 in (*22*)]. Our measurements at that height match this model value at the end of the time range analyzed, after the decay of the magnetic field is over, which implies that the magnetic field in the flare evolves toward an equilibrium state. However, the much stronger values observed earlier in the flare are several times as high as the equilibrium values. This indicates that a dynamic, transient magnetic field was lifted up from lower heights by the eruption process. This redistribution of the strong magnetic field—originally located low in the corona—over a much larger coronal volume during the flare might power the solar flare and associated eruption.

The Faraday equation is $\dot{\mathbf{B}} = -c\nabla \times \mathbf{E}$ (where **B** and **E** are the magnetic and electric field vectors, respectively, and c is the speed of light), which requires that an electric field be associated with the observed decay in magnetic field strength. Estimating $|\nabla \times \mathbf{E}|$ as E/R, where R is the scale of nonuniformity at the cusp region, and adopting representative values $\dot{B} \approx 5\,\mathrm{G\,s^{-1}}$ and $R \approx 3.65 \times 10^8$ cm—equivalent to 5 arc sec on the Sun, which is the size of the smallest coherent structures in the magnetic maps [as well as in extreme ultraviolet (EUV) images (*15*)]—we find $E \sim 20\,\mathrm{V\,cm^{-1}}$. For comparison, the Dreicer field, which demarcates regimes of the steady electric current and free runaway of the plasma electrons (*23*), is $E_D \sim 10^{-4}\,\mathrm{V\,cm^{-1}}$. This field strength E is consistent, within an order of magnitude, with available indirect estimates (*10*, *24*, *25*) for other large flares. Our choice of the scale $R \approx 5$ arc sec is ~10 to 20% of the cusp size and represents the macroscopic structure. It does not preclude the existence of smaller-scale structures and the proportionally smaller electric fields associated with them. However, the derived electric field remains above the Dreicer value for any scales $\gtrsim 5 \times 10^{-5}$ arc sec.

The decrease in magnetic energy at the cusp region must be associated with a conversion of that energy into other forms. An energy source is needed at the cusp region of this event to account for its enhanced temperature (*15*). The magnetic-field–aligned component of our inferred electric field should accelerate particles as required to power the microwave emission and could drive the observed enhanced heating at the cusp region (*15*).

The decay in magnetic field strength implies advection and/or diffusion of the magnetic field, which can be estimated using the induction equation, $\dot{\mathbf{B}} = \nabla \times [v \times \mathbf{B}] + \nu\nabla^2\mathbf{B}$, where v is the plasma velocity and ν is the magnetic diffusivity. The advection term, $\nabla \times [v \times \mathbf{B}]$, can easily account for the magnetic field variation during the phase of apparent upward motion of the arclike structures in the magnetic field maps from 15:57:00 to 15:59:25 UTC (movie S1). However, at later times these arclike structures fade without moving, which implies dissipation of the magnetic field, not advection. We estimate the magnetic diffusivity ν required to drive the apparent decay rate ($|\dot{B}| \approx 5\,\mathrm{G\,s^{-1}}$) of the magnetic field ($B \approx 600$ G) as $\nu \sim R^2\,\dot{B}/B \sim 10^{15}\,\mathrm{cm^2\,s^{-1}}$. This value of ν is much larger than the magnetic diffusivity due to Coulomb collisions (*26*). It can only be provided by turbulent magnetic diffusion, which appears when a large fraction of the velocity v entering the induction equation is fluctuating [turbulent-like (*27*)], rather than steady. Averaging the induction equation over the random velocity field results in a renormalization of the magnetic diffusivity coefficient (*26*) such that $\nu \sim u\,R/3$, where u is the typical turbulent velocity. Nonthermal turbulent velocities of $u \sim 100\,\mathrm{km\,s^{-1}}$ were measured at the cusp region in this flare (*15*), which implies $\nu \sim u\,R/3 \sim 1.2 \times 10^{15}\,\mathrm{cm^2\,s^{-1}}$, in agreement with the estimate obtained from $\dot{B}$ above.

Figure 3B shows the evolution of the mean magnetic energy density (*13*) in this region. Over ~1.5 min, the magnetic energy density decays at a rate of ~200 erg $\mathrm{cm^{-3}\,s^{-1}}$, losing ~80% of the magnetic energy available in this area. The net decrease of the magnetic energy in the adopted nominal flare volume of $10^{28}\,\mathrm{cm^3}$, which corresponds to a source with a linear scale of ~20 Mm (Fig. 1), is ~2×10^{32} erg.

We compare this reduction in magnetic energy density with the energy density of nonthermal electrons (microwave diagnostics provides the instantaneous electron and energy densities, unlike x-ray diagnostics, which provides electron and energy flux), which we compute from the same data (*13*). Figure 3B

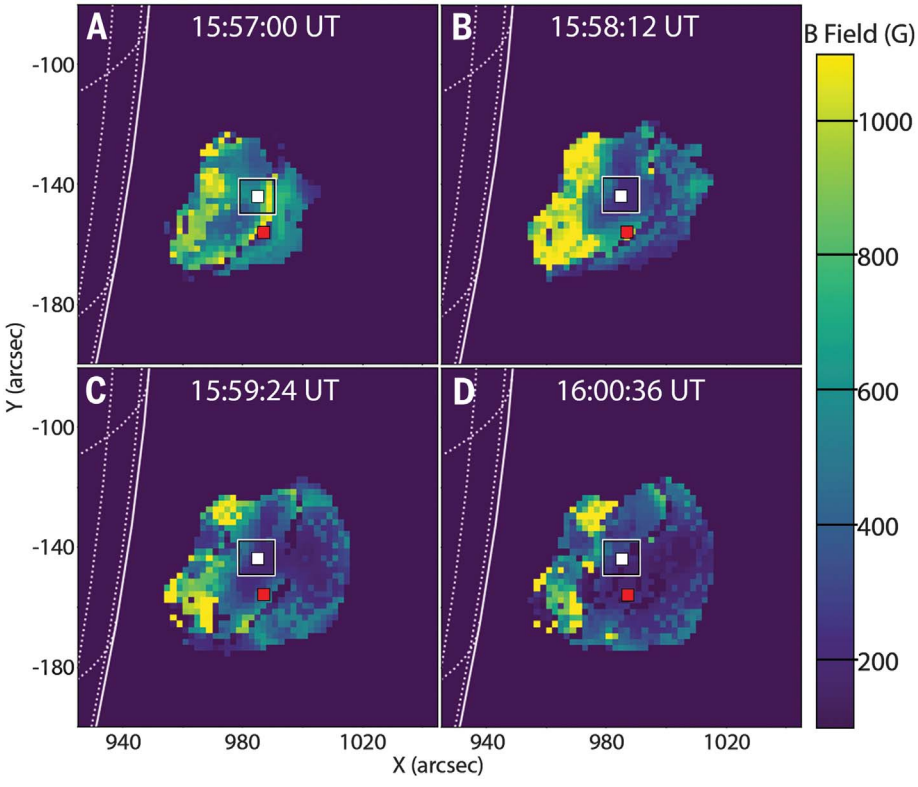

Fig. 2. Evolving maps of the coronal magnetic field. (**A** to **D**) Four coronal magnetic field maps derived for the 10 September 2017 flare, separated by 72 s. Apparent upward motion of the radio source and looplike structures in the magnetic field maps is visible in panels (A) to (C), showing the spreading of the reconnection process upward. Red and white squares, and the empty white box, correspond to locations shown in Fig. 3. The solar coordinate grid and the solar photosphere are shown by the white dotted and solid lines, respectively. Movie S1 shows an animated version of this figure.

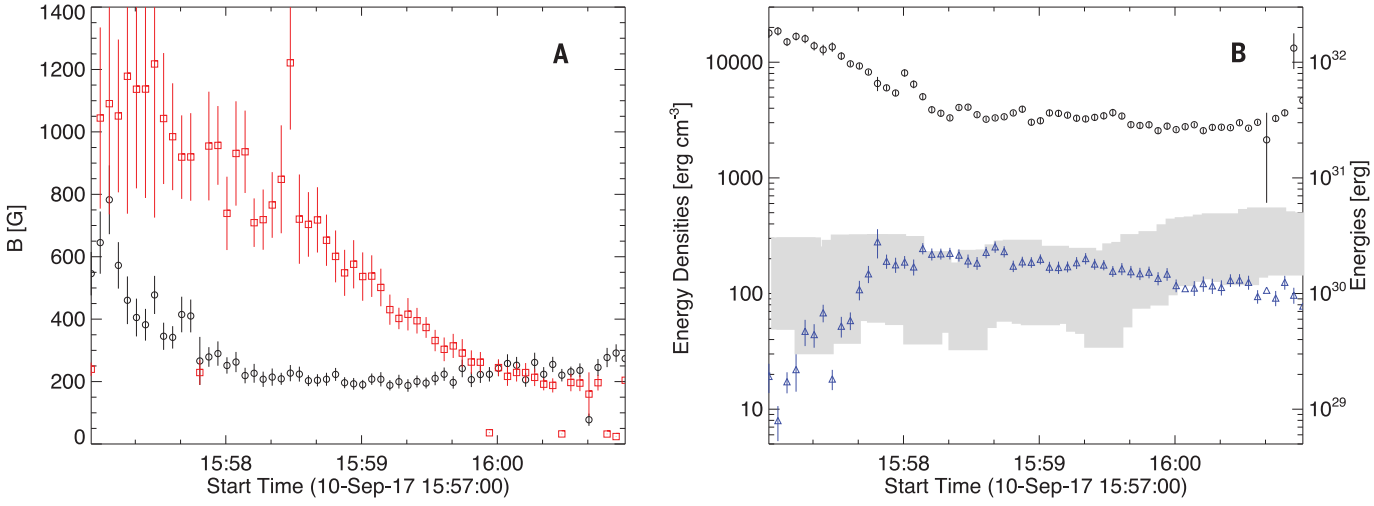

Fig. 3. Evolution of the magnetic field and magnetic energy. (**A**) Evolution of the magnetic field at two locations shown in Fig. 2. The red and black symbols show the data from the red and white squares, respectively. Black circles show decay of the magnetic field from 15:57 to 15:58 UTC, remaining roughly constant after that. The red squares, which correspond to a higher member of the system of nested loops, show a similar decay lasting 2 min longer, coinciding with the apparent upward motion of the EUV loops (Fig. 2). Error bars show 1σ uncertainties. (**B**) The mean magnetic energy density w_B (black circles) and the mean energy density of nonthermal electrons w_{nth} (blue triangles), both computed within the white box shown in Fig. 2. The shaded gray area indicates our estimated range of thermal energy density computed in (*13*). The right axis shows the corresponding total energy, assuming a flare volume of 10^{28} cm^3. Error bars show 1σ uncertainties.

shows the evolution of the (lower bound of the) nonthermal energy density, assuming a power-law distribution of electrons with a low-energy cutoff of E_{min} = 20 keV (*13*). Although this nonthermal energy constitutes only a few percent of the decrease in magnetic energy, it appears that the main decay of the magnetic energy is correlated in time with the increase of the nonthermal electron energy. This result implies that a direct energy conversion occurs in this region. The thermal energy density and kinetic energy density of turbulent motions cannot be estimated from the microwave diagnostics alone but require additional inputs based on available EUV diagnostics (*15*). The estimated thermal energy density (*13*) is also shown in Fig. 3B. It overlaps with the lower bound of the nonthermal energy density obtained above. The kinetic energy associated with random motions of the plasma is two orders of magnitude lower than the thermal energy. This implies that we observe a region at the cusp location—where available magnetic energy is converted to other forms of flare energy—which occurs below, but not within, the reconnection current sheet. The observed release of the magnetic energy is sufficient to power all other observed forms of energy in the flare.

Our observations quantify the coronal magnetic energy at the flare site and establish exactly where and how fast it is released. Our findings provide a quantitative observation of energy transformation in a solar flare, linking the thermal and nonthermal energy components to the associated magnetic energy release.

REFERENCES AND NOTES

1. T. Yokoyama, K. Shibata, *Nature* **375**, 42–44 (1995).
2. B. Kliem, T. Török, *Phys. Rev. Lett.* **96**, 255002 (2006).
3. K. Shibata *et al.*, *Science* **318**, 1591–1594 (2007).
4. S. Scaringi, T. J. Maccarone, C. D'Angelo, C. Knigge, P. J. Groot, *Nature* **552**, 210–213 (2017).
5. P. F. Wyper, S. K. Antiochos, C. R. DeVore, *Nature* **544**, 452–455 (2017).
6. H. Carmichael, in *The Physics of Solar Flares, Proceedings of the AAS-NASA Symposium held 28-30 October, 1963 at the Goddard Space Flight Center, Greenbelt, MD*, W. N. Hess, Ed. (National Aeronautics and Space Administration, 1964), vol. 50, p. 451.
7. P. A. Sturrock, *Nature* **211**, 695–697 (1966).
8. T. Hirayama, *Sol. Phys.* **34**, 323–338 (1974).
9. R. A. Kopp, G. W. Pneuman, *Sol. Phys.* **50**, 85 (1976).
10. E. Priest, T. Forbes, *Magnetic Reconnection* (Cambridge Univ. Press, 2007).
11. X. Sun *et al.*, *Astrophys. J.* **748**, 77 (2012).
12. M. L. DeRosa *et al.*, *Astrophys. J.* **696**, 1780–1791 (2009).
13. Materials and methods are available as supplementary materials.
14. Y. Li *et al.*, *Astrophys. J.* **853**, L15 (2018).
15. H. P. Warren *et al.*, *Astrophys. J.* **854**, 122 (2018).
16. D. E. Gary *et al.*, *Astrophys. J.* **863**, 83 (2018).
17. N. Omodei, M. Pesce-Rollins, F. Longo, A. Allafort, S. Krucker, *Astrophys. J.* **865**, L7 (2018).
18. D. M. Long *et al.*, *Astrophys. J.* **855**, 74 (2018).
19. G. A. Doschek *et al.*, *Astrophys. J.* **853**, 178 (2018).
20. D. Longcope, J. Unverferth, C. Klein, M. McCarthy, E. Priest, *Astrophys. J.* **868**, 148 (2018).
21. G. M. Nita, J. Hickish, D. MacMahon, D. E. Gary, *J. Astron. Instrum.* **05**, 1641009 (2016).
22. S. A. Anfinogentov, A. G. Stupishin, I. I. Mysh'yakov, G. D. Fleishman, *Astrophys. J.* **880**, L29 (2019).
23. H. Dreicer, *Phys. Rev.* **115**, 238–249 (1959).
24. J. Qiu, D. E. Gary, G. D. Fleishman, *Sol. Phys.* **255**, 107–118 (2009).
25. G. D. Fleishman *et al.*, *Astrophys. J.* **822**, 71 (2016).
26. G. D. Fleishman, I. N. Toptygin, *Cosmic Electrodynamics: Electrodynamics and Magnetic Hydrodynamics of Cosmic Plasmas* (Springer 2013).
27. J. T. Dahlin, J. F. Drake, M. Swisdak, *Phys. Plasmas* **24**, 092110 (2017).

ACKNOWLEDGMENTS

We thank the scientists and engineers who helped design and build EOVSA, especially G. Hurford, S. White, J. McTiernan, W. Grammer, and K. Nelin. **Funding:** This work was supported in part by NSF grants AGS-1817277, AST-1910354, and AGS-1654382 and NASA grants NNX17AB82G, 80NSSC18K0667, 80NSSC19K0068, and 80NSSC18K1128 to the New Jersey Institute of Technology. N.K. was partially supported by the NASA Living With a Star Jack Eddy Postdoctoral Fellowship Program, administered by UCAR's Cooperative Programs for the Advancement of Earth System Science (CPAESS). **Author contributions:** G.D.F. developed the methodology, performed the model fitting, analyzed the results, and wrote the draft manuscript; D.E.G. led the construction and commissioning of the EOVSA and developed the observational strategy and calibration for microwave spectroscopy; B.C. developed the microwave spectral imaging and self-calibration strategy; N.K. wrote software used in the analysis and visualization; D.E.G., B.C., and S.Y. prepared the microwave observation data; S.Y. implemented the microwave imaging pipeline under the guidance of D.E.G. and B.C.; and G.M.N. developed software used in modeling and testing the spectral fitting methodology and developed the GSFIT spectral fitting package. All authors discussed the interpretation of the data, contributed scientific results, and helped prepare the paper. **Competing interests:** The authors declare no competing interests. **Data and materials availability:** Raw EOVSA observational data used for this study are available at www.ovsa.njit.edu/fits/IDB/20170910/IDB20170910155625/. Fully processed EOVSA spectral imaging data (in IDL save format) are available at http://ovsa.njit.edu/publications/fleishman_ea_science_2019/data/. The microwave data fitting software, GSFIT, is available in the community-contributed SolarSoftWare repository, under the packages category, at www.lmsal.com/solarsoft/ssw/packages/gsfit/.

SUPPLEMENTARY MATERIALS

science.sciencemag.org/content/367/6475/278/suppl/DC1
Materials and Methods
Figs. S1 and S2
References (*28*–*33*)
Movies S1 and S2

13 April 2019; accepted 4 December 2019
10.1126/science.aax6874

Decay of the coronal magnetic field can release sufficient energy to power a solar flare

Gregory D. Fleishman, Dale E. Gary, Bin Chen, Natsuha Kuroda, Sijie Yu and Gelu M. Nita

Science **367** (6475), 278-280.
DOI: 10.1126/science.aax6874

Magnetic energy release in a solar flare

Solar flares are bright flashes and associated eruptions of plasma from the Sun that are thought to be powered by violent rearrangement of the magnetic fields near sunspots. Fleishman *et al.* observed a bright solar flare with a microwave interferometer, allowing them to map the magnetic field in the solar corona and monitor how it changed during the flare. They found a large drop in the local field strength over 2 minutes, releasing enough magnetic energy to power the entire solar flare. Determining the origin of this energy will help to predict how strong future solar flares may be and their potential space weather impacts on Earth.

Science, this issue p. 278